Plasmon-assisted low-threshold nanolasers

Yu-Wei Lu ⬤

School of Physics and Optoelectronic Engineering, Foshan University, Foshan 528000, China
and School of Physics and Optoelectronics, South China University of Technology, Guangzhou 510641, China

Wei Li

State Key Laboratory of Optoelectronic Materials and Technologies, School of Physics,
Sun Yat-sen University, Guangzhou 510275, China

Renming Liu ⬤

Institute of Photobiophysics, School of Physics and Electronics, Henan University, Kaifeng 475004, China

Yanxiong Wu and Haishu Tan[*]

School of Physics and Optoelectronic Engineering, Foshan University, Foshan 528000, China

Yongyao Li[†]

School of Physics and Optoelectronic Engineering, Foshan University, Foshan 528000, China
and Guangdong-Hong Kong-Macao Joint Laboratory for Intelligent
Micro-Nano Optoelectronic Technology, Foshan University, Foshan 528000, China

Jing-Feng Liu ⬤

College of Electronic Engineering, South China Agricultural University, Guangzhou 510642, China

Low power consumption is of great importance for on-chip optical applications of nanolasers. To reduce the lasing threshold, a high quality factor and strong Purcell effect are vital, while the latter is often hindered by the above-diffraction-limit mode volume of photonic cavity, and its improvement generally requires complicated cavity design. We show that by coupling to an off-resonant plasmonic antenna, the lasing threshold of a photonic cavity can be reduced over a wide range of parameters where the plasmon-assisted coherent light-matter interaction dominates over the plasmon-induced dissipation. We develop a semiclassical model of a two-level nanolaser for such a hybrid plasmonic-photonic cavity, which is consistent with the quantum description of the spectral density of a hybrid cavity. The analytical expression of the lasing threshold is derived, which can be utilized to optimize the system parameters associated with cavities designed to obtain the minimum lasing threshold. Through comprehensive study, we find that compared to all-dielectric photonic cavity, a hybrid cavity can have prominent advantages in lasing with lower threshold, narrower emission linewidth, and sustaining the higher-power output of laser field. Our paper demonstrates the possibility of utilizing a hybrid plasmonic-photonic cavity to fabricate room-temperature low-threshold nanolasers.

I. INTRODUCTION

A fast, compact, and power-efficient coherent light source at nanoscale is highly desirable for a variety of practical applications, ranging from integrated optical circuits [1–3] and near-field spectroscopy [4,5] to biological nanoprobe [6,7]. Since early demonstrations [8,9], reducing the lasing threshold has been one of the primary research goals of nanolasers. In the last decade, great efforts have been devoted to exploiting the high Q-factor dielectric photonic structures for low

energy loss, like microdisks [1,10], photonic crystal (PhC) slabs [11,12] and various periodical arrays [13–15]. Besides the intrinsic dissipation of a cavity, the lasing threshold also depends on the β factor, the fraction of spontaneous emission (SE) directed into a lasing mode [16]. A large β factor mainly results from the strong Purcell effect, meaning a strong feedback between the lasing mode and the gain medium, and hence the low lasing threshold. However, the Purcell factor of a photonic cavity is limited by the mode volume, for at least one dimension of dielectric cavity is comparable to the resonant wavelength. Another technical route is found to realize the metal-based nanolasers that utilize the surface plasmon resonance of plasmonic resonators, called spasers [7,17–19]. Spasers exhibit a physical size down to tens of

[*]tanhaishu@fosu.edu.cn
[†]yongyaoli@gmail.com

nanometers in all dimensions and a Purcell factor exceeding 10^6 [20,21]. Nevertheless, this extreme light confinement far below the diffraction limit is achieved by transferring the electrical energy into the kinetic energy of free electrons in metal, thus at the price of high nonradiative dissipation and low Q factor [22]. Furthermore, strong quenching effect due to the mode overlap between the dipolar mode and the higher order modes results in a poor β factor [20,23–25]. These reverse the advantage of strong Purcell effect in plasmonic resonators and lead to a high lasing threshold and wide linewidth, in spite of fs switching time [22].

Recent progress in the exploration of hybrid plasmonic-photonic cavities demonstrates the possibility of combining the advantages of both kinds of cavities, with enhanced coherent light-matter interaction between the photonic mode and the quantum emitter (QE) while avoiding the unwanted dissipation in metal [26–29]. The maximum Purcell rate of transfer of population from QE to cavity mode can be found at large plasmon-photon detuning, resulting from the trade-off between the plasmon-induced field confinement and dissipation [26,30–32]. Therefore, plasmonic antennas can realize the threshold reduction of dielectric nanolasers without the demanding requirement of high Q factor and small mode volume.

To understand the technical characteristic of lasing action in the novel hybrid plasmonic-photonic cavity, a flexible and physically transparent nanolaser model will be beneficial, while to the best of our knowledge, is still lacking. The aim of this paper is to develop a generalized semiclassical laser theory for a plasmonic-photonic cavity and compare the lasing characteristics with an all-dielectric microcavity.

The rest of paper is organized as follows. In Sec. II, we present the semiclassical two-level laser theory for a hybrid cavity with large plasmon-photon detuning. The minimum lasing threshold and steady-state photon number are analytically obtained. Section III is devoted to comparing the lasing characteristics of a hybrid cavity and bare microcavity. Section IV demonstrates the lasing threshold reduction of a realistic hybrid cavity. We conclude in Sec. V. The technical details are given in the Appendixes.

II. SEMICLASSICAL NANOLASER THEORY OF PLASMONIC-PHOTONIC CAVITY

The basic model of a two-level nanolaser is illustrated in Fig. 1(a). We consider a dipolar plasmonic antenna since the higher-order modes are nonradiative, then the plasmonic-photonic cavity can be treated as two coupled single-mode cavities with coupling strength g_1 [26,32]. This hypothesis is justified for plasmonic dimers [33,34] and common elongate monomers like plasmonic rods [35,36] and ellipsoids [37], whose dipolar mode are often well separated from the higher-order modes. The gain medium is considered an ensemble of N incoherently pumped two-level QEs. The kth QE couples to the photonic mode of the microcavity and the plasmonic mode of antenna with coupling strengths g_c^k and g_a^k, respectively.

The full Hamiltonian of the system under the rotating wave approximation (RWA) can be written as
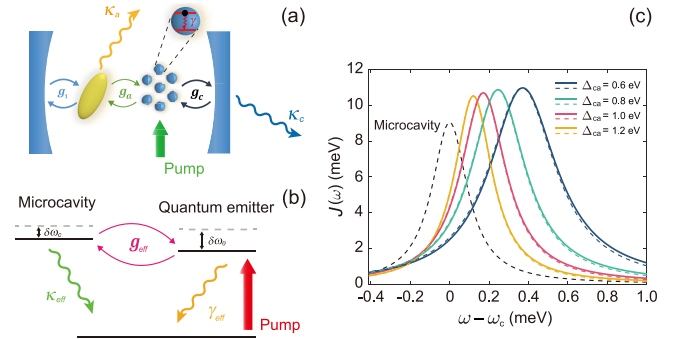
$$H = H_0 + H_I, \tag{1}$$

FIG. 1. (a) Schematic of the two-level nanolaser model for hybrid cavity constituted of the interacting plasmonic antenna and microcavity. (b) Sketch of the effective interaction between the microcavity and the QE after eliminating the plasmonic modes. (c) Spectral density for various plasmon-photon detuning Δ_{ca}, with the parameters $V_m = 4 \times 10^3$ nm^3 and $V_c = 0.01$ μm^3. The solid and dashed lines show the spectral density of the effective model and the cQED model, respectively. Other parameters are mentioned in the text.

with the free Hamiltonian

$$H_0 = \omega_a a^\dagger a + \omega_c c^\dagger c + \omega_0 \sum_k^N \sigma_+^k \sigma_-^k \tag{2}$$

and the interaction Hamiltonian

$$H_I = \sum_k^N g_a^k (a^\dagger \sigma_-^k + \sigma_+^k a) + \sum_k^N g_c^k (c^\dagger \sigma_-^k + \sigma_+^k c) + g_1 (a^\dagger c + a c^\dagger), \tag{3}$$

which describes the closed-loop coupling between the plasmonic mode, the photonic mode, and the QEs. a and c are the bosonic annihilation operators for the plasmonic mode and the photonic mode, respectively, with resonance frequencies ω_a and ω_c. $\sigma_-^k = |g\rangle\langle e|$ denotes the lowering operator of the kth QE. QEs are assumed to have the same transition frequency ω_0. The system dynamics follows the quantum master equation (QME),

$$\frac{\partial \rho}{\partial t} = i[\rho, H] + \frac{\gamma_{//} P}{2} \mathcal{L}_{\sigma_+}(\rho) + \frac{\gamma_{//}}{2} \mathcal{L}_{\sigma_-}(\rho) + \frac{\gamma_p}{2} \mathcal{L}_{\sigma_z}(\rho) + \frac{\kappa_a}{2} \mathcal{L}_a(\rho) + \frac{\kappa_c}{2} \mathcal{L}_c(\rho), \tag{4}$$

where $\mathcal{L}_{\hat{o}}(\rho) = 2\hat{o}\rho\hat{o}^\dagger - \hat{o}^\dagger\hat{o}\rho - \rho\hat{o}^\dagger\hat{o}$ is the Liouvillian superoperator for operator $\hat{o}$. $\gamma_{//}$ is the SE rate of QEs into modes other than the plasmonic and photonic modes, and $\gamma_{//} P$ stands for the incoherent pump rate. γ_p represents the dephasing rate of QEs and κ_a/κ_c is the decay rate of plasmonic/photonic mode. From the QME, we can obtain the following equations of motion:

$$\langle \dot{a} \rangle = -i\left(\omega_a - i\frac{\kappa_a}{2}\right)\langle a \rangle - i\sum_k^N g_a^k \langle \sigma_-^k \rangle - ig_1\langle c \rangle, \tag{5}$$

$$\langle \dot{c} \rangle = -i\left(\omega_c - i\frac{\kappa_c}{2}\right)\langle c \rangle - i\sum_k^N g_c^k \langle \sigma_-^k \rangle - ig_1\langle a \rangle, \tag{6}$$

$$\langle \dot{\sigma}_-^k \rangle = -i\Big(\omega_0 - i\frac{\gamma_\perp}{2}\Big)\langle\sigma_-^k\rangle + ig_a^k\langle\sigma_z^k\rangle\langle a\rangle + ig_c^k\langle\sigma_z^k\rangle\langle c\rangle, \quad (7)$$

$$\langle\dot{\sigma}_z^k\rangle = 2ig_a^k(\langle a^\dagger\rangle\langle\sigma_-^k\rangle - \langle\sigma_+^k\rangle\langle a\rangle)$$
$$+ 2ig_c^k(\langle c^\dagger\rangle\langle\sigma_-^k\rangle - \langle\sigma_+^k\rangle\langle c\rangle)$$
$$+ \gamma_{//}P(1 - \langle\sigma_z^k\rangle) - \gamma_{//}(\langle\sigma_z^k\rangle + 1), \quad (8)$$

where $\gamma_\perp = 2\gamma_p + \gamma_{//}(P+1)$ is the QE polarization decay. We have neglected the QE-field correlation by factorizing the second-order expectation values $\langle\sigma_z^k c\rangle$, $\langle c^\dagger\sigma_-^k\rangle$, and $\langle\sigma_+^k c\rangle$ into the products of the first-order expectation values $\langle\sigma_z^k\rangle\langle c\rangle$, $\langle c^\dagger\rangle\langle\sigma_-^k\rangle$, and $\langle\sigma_+^k\rangle\langle c\rangle$, respectively.

Previous studies reported the enhanced coherent light-matter interaction in a hybrid cavity with red-detuned plasmonic-photonic coupling ($\omega_a > \omega_c$) [26,38,39], which is also the regime we focus on in this paper. In the case of resonant or nearly resonant QE-cavity coupling, i.e., $|\Delta_{ca}| = |\omega_a - \omega_c| \gg |\Delta_{0c}| = |\omega_c - \omega_0|$, lasing only occurs at the photonic mode due to the high dissipation of plasmonic mode and the large detuning from gain medium. In this case, the intensity of the laser field in the photonic mode dominates over the plasmonic mode. Therefore, the plasmonic mode can be considered an auxiliary mode. By formally integrating Eq. (5) and applying the Markovian approximation, we find (see Appendix A for more details)

$$\langle a\rangle \approx -\frac{\sum_k^N g_a^k}{(\omega_a - \omega_0) - i\frac{\kappa_a}{2}}\langle\sigma_-^k\rangle - \frac{g_1}{(\omega_a - \omega_c) - i\frac{\kappa_a}{2}}\langle c\rangle. \quad (9)$$

Plugging back into Eqs. (6)–(8), we can eliminate the plasmonic mode and obtain the modified Maxwell-Bloch (MB) equations in the semiclassical limit,

$$\langle\dot{\sigma}_-^k\rangle = -i\Big(\omega_0'^k - i\frac{\gamma_{\text{eff}}^k}{2}\Big)\langle\sigma_-^k\rangle + ig_{\text{eff}}^k\langle\sigma_z^k\rangle\langle c\rangle, \quad (10)$$

$$\langle\dot{c}\rangle = -i\Big(\omega_c' - i\frac{\kappa_{\text{eff}}}{2}\Big)\langle c\rangle - i\sum_k g_{\text{eff}}^k\langle\sigma_-^k\rangle, \quad (11)$$

$$\langle\dot{\sigma}_z^k\rangle = 2i\big(g_{\text{eff}}^{k*}\langle c^\dagger\rangle\langle\sigma_-^k\rangle - g_{\text{eff}}^k\langle\sigma_+^k\rangle\langle c\rangle\big)$$
$$- \big(\gamma_{//} + \gamma_m^k\big)\big(\langle\sigma_z^k\rangle + 1\big) + \gamma_{//}P\big(1 - \langle\sigma_z^k\rangle\big), \quad (12)$$

where $\omega_0'^k = \omega_0 + \delta\omega_0^k$ and $\omega_c' = \omega_c + \delta\omega_c$ are the modified frequencies of the kth QE and lasing mode, respectively, with $\delta\omega_0^k = -|g_a^k|^2\Delta\omega_0/|\Delta_0|^2$ and $\delta\omega_c = g_1^2\Delta\omega_c/|\Delta_c|^2$ being the frequency shifts due to the perturbation of plasmonic mode, where $\Delta_X = \Delta\omega_X - i\kappa_a/2$ with $\Delta\omega_X = \omega_a - \omega_X$ being the frequency detuning and indices $X = c, 0$. $g_{\text{eff}}^k = g_c^k - g_a^k g_1/\Delta_c$ is the effective coupling strength between the lasing mode and the QE, which is complex-valued, and its imaginary part represents the plasmon-mediated dissipative interaction. The effective decay rates of lasing mode and QE are $\kappa_{\text{eff}} = \kappa_c + \kappa_m$ and $\gamma_{\text{eff}}^k = \gamma_\perp + \gamma_m^k$, respectively, where $\kappa_m = g_1^2\kappa_a/|\Delta_c|^2$ and $\gamma_m^k = |g_a^k|^2\kappa_a/|\Delta_0|^2$ are the plasmon-induced decay rates. The modified MB Eqs. (10)–(12) have the same form as the MB equations of a single-mode cavity [16,19], but replace the original decay rates and coupling strength by the effective parameters γ_{eff}^k, κ_{eff}, and g_{eff}^k, and thus describe the effective interaction between the lasing mode and the QEs, as Fig. 1(b) depicts. Particularly, the complex-valued g_{eff}^k indicates that what distinguishes the hybrid cavity

from a single-mode cavity is that the plasmon-mediated QE-cavity interaction demonstrates both coherent and dissipative characteristics. It also indicates that the plasmonic mode enhances the magnitude of QE-cavity coupling strength by a factor $\alpha = 1 + |g_1 g_a/g_c\Delta_c|$, which is mainly contributed by the coherent component for large plasmonic-photonic detuning.

In MB equations, the lasing threshold is mainly determined by the cavity decay rate and the coupling strength between the gain medium and the lasing mode. These two parameters of a cavity can be extracted from the spectral density, which fully governs the interaction of a QE with an arbitrary electromagnetic (EM) environment [40]. For a single-mode cavity, in general, the spectral density presents a Lorentzian line shape, while the hybrid cavity is non-Lorentzian [26,38,41,42]. However, since the modified MB equations have the same form as the MB equations of a single-mode cavity, the spectral density of effective interaction in plasmonic-photonic cavity is still the standard Lorentzian function:

$$J_{\text{eff}}(\omega) = |g_{\text{eff}}|^2\frac{\kappa_{\text{eff}}/2}{(\omega - \omega_c')^2 + (\kappa_{\text{eff}}/2)^2}. \quad (13)$$

On the other hand, the exact spectral density of a hybrid cavity can be analytically derived from the cavity quantum-electrodynamics (cQED) model (see Appendix C for a detailed derivation), which yields

$$J(\omega) = -g_c^2\,\text{Im}\,[J_c(\omega)] - 2g_a g_c\,\text{Im}\,[J_{ac}(\omega)] - g_a^2\,\text{Im}\,[J_a(\omega)], \quad (14)$$

with

$$J_X(\omega) = \chi_X(\omega)\big[1 - g_1^2\chi_a(\omega)\chi_c(\omega)\big]^{-1}, \quad (15)$$

$$J_{ac}(\omega) = g_1\chi_a(\omega)\chi_c(\omega)\big[1 - g_1^2\chi_a(\omega)\chi_c(\omega)\big]^{-1}, \quad (16)$$

where $\chi_X(\omega) = [(\omega - \omega_X) + i\kappa_X/2]^{-1}$ for $X = a, c$. Figure 1(c) compares $J_{\text{eff}}(\omega)$ with $J(\omega)$ around the resonance frequency of the lasing mode for $\Delta_{ca} \geqslant 0.6\,\text{eV}$, where it shows good accordance between two models since in this case $J(\omega)$ approximates the Lorentzian line shape. Therefore, the modified MB equations can accurately describe the lasing action in hybrid cavity in the case of large plasmonic-photonic detuning.

The modified MB equations always have a trivial zero solution, while the nontrivial solution corresponds to the lasing action, which can be found from the characteristic matrix of Eqs. (10) and (11),

$$\begin{pmatrix} \omega_c' + \Delta_{c0} - i\frac{\gamma_{\text{eff}}}{2} - \omega_s & -ge^{i\theta}\langle\sigma_z^s\rangle \\ Nge^{i\theta} & \omega_c' - i\frac{\kappa_{\text{eff}}}{2} - \omega_s \end{pmatrix}, \quad (17)$$

where we let $g_{\text{eff}} \equiv ge^{i\theta}$. ω_s is the lasing frequency and $\Delta_{c0} = \omega_0' - \omega_c'$ stands for the frequency detuning between the QE and the lasing mode. By separating the real and imaginary parts of the above characteristic matrix and setting to zero [43], we can find that the minimum steady-state population inversion is $\langle\sigma_z^s\rangle = \kappa_{\text{eff}}\gamma_{\text{eff}}/4Ng^2\cos^2(\theta)$, which yields the minimum lasing threshold, achieved at $\Delta_{c0} = (\gamma_{\text{eff}} - \kappa_{\text{eff}})\tan(\theta)/2$; the lasing frequency is determined as $\omega_s = \omega_c' - \kappa_{\text{eff}}\tan(\theta)/2$ (see details in Appendix B). On the other hand,

Eqs. (10) and (12) give the steady-state photon number,

$$n_c \equiv |c|^2 = n_{\text{sat}}^{-1} \frac{(1 - \langle \sigma_z^s \rangle)(P + v_m) - 2v_m}{\langle \sigma_z^s \rangle}, \quad (18)$$

where $v_m = 1 + \gamma_m/\gamma_{//}$ and the saturation photon number $n_{\text{sat}} = 8g^2 \cos(\theta)^2/\gamma_{//}\gamma_{\text{eff}}$. It is worth noting that $g\cos(\theta)$ is the real part of g_{eff}, and thus represents the magnitude of the coherent component of the effective QE-cavity interaction. It implies that the lasing is only determined by the coherent light-matter interaction, which distinguishes from the quantum dynamics of QE interacting with hybrid cavity, where the dissipative interaction is crucial for manipulating the quantum states of system [31,32,44].

From Eq. (18), the population inversion at lasing threshold can be found by letting $n_c = 0$; the solution is $\langle \sigma_z^{\text{th}} \rangle = (P_{\text{th}} - v_m)/(P_{\text{th}} + v_m)$. Equating $\langle \sigma_z^{th} \rangle$ with $\langle \sigma_z^s \rangle$, we can obtain the analytical expression of the lasing threshold,

$$P_{\text{th}}/\gamma_{//} = \bar{n} - v_s - \sqrt{(\bar{n} - v_s)^2 - v_m[2\bar{n} + (v_s + v_p)]}, \quad (19)$$

where $v_s = v_m + v_p$, $v_p = \gamma_p/\gamma_{//}$, and $\bar{n} = NC_{\text{eff}}/\gamma_{//}$, with $C_{\text{eff}} = 2g^2 \cos(\theta)^2/\kappa_{\text{eff}}$ being the effective Purcell rate of transfer of population from QE to the lasing mode [45]. For nanolasers, in general $\bar{n}, v_p \gg 1$, the second term in the radical sign is a small quantity, and thus the lasing threshold can be approximately expressed as $P_{\text{th}}/\gamma_{//} \approx v_m(\bar{n} + v_p)/(\bar{n} - v_p)$; while the threshold of a single-mode cavity is $P_{\text{th}}^0/\gamma_{//} = (\bar{n}_0 + v_p)/(\bar{n}_0 - v_p)$ [16,19], where $\bar{n}_0 = NC_0/\gamma_{//}$ with $C_0 = 2g_c^2/\kappa_c$. By comparing with P_{th}^0, the physical meaning of P_{th} is clear: the plasmonic antenna constitutes nonlasing modes, and thus the lasing threshold is scaled as v_m and linearly increased with the plasmon-induced QE decay; on the other hand, the coherent interaction between the QE and the lasing mode is enhanced through the plasmonic antenna, but the decay of lasing mode increases as well. Therefore, the coupling of a microcavity to a plasmonic antenna is not always beneficial to lasing. Note that both the effective coupling strength g_{eff} and dissipation κ_m, γ_m are related to Δ_{ca} and become greater as Δ_{ca} decreases. Therefore, the plasmon-photon detuning Δ_{ca} plays an important role in determining the lasing threshold.

III. LASING CHARACTERISTICS

We first consider a prototype model to investigate the lasing action of hybrid cavity. The quality factor of the microcavity is taken as 10^4 considering the material absorption, and we choose a gold nanoparticle as the plasmonic antenna. The permittivity of gold is described by the Drude model $\varepsilon_m(\omega) = \varepsilon_\infty - \omega_{pl}^2/(\omega^2 + i\omega\gamma_{pl})$, where $\varepsilon_\infty = 1$ is the constant background permittivity, $\omega_{pl} = 4$eV is the resonance frequency, and $\gamma_{pl} = 0.2$ eV represents the collision rate [32]. The dipole moment of the QE is $\mu = 1e \times$ nm [46–48]. The SE rate of QE is evaluated as $\gamma_{//} \approx 0.1$ meV, which takes into account the radiation to higher order modes of plasmonic antenna. The dephasing rate $\gamma_p = 15$ meV corresponds to the typical linewidth of QE at room temperature [23,47,49]. It is worth noting that the coupling strengths g_c, g_a, and g_1 are not independent parameters but determined by the mode volumes of microcavity (V_c) and plasmonic antenna (V_m); see

Appendix D for the relation between the coupling strength and the mode volume of optical resonator. Therefore, in the following study, we investigate the lasing action in terms of mode volumes instead of coupling strengths. The minimum mode volume of the PhC microcavity is given by $V_c \sim (\lambda/2n)^3$, where λ and n are the free-space wavelength and the refractive index of the medium, respectively. While for PhC slab [50], nanobeam [51,52], and whispering-gallery-mode (WGM) microcavities [26,42,53], the mode volume will be larger without elaborate design [54], which is typically on the order of $(\lambda/n)^3$. The mode volume of the plasmonic antenna ranges from 10^4 nm^3 to below 10^2 nm^3, according to different shapes [26,35,55].

Figure 2(a) shows the lasing threshold of hybrid cavity as the function of plasmonic mode volume V_m and plasmon-photon detuning Δ_{ca} with 40 QEs, normalized by that of a bare microcavity. The mode volume of microcavity $V_c = 0.15 \mu$m^3 corresponds to $g_c = 0.31$ meV. An optimal parameter $(V_m, \Delta_{ca}) = (1.8 \times 10^4$ nm^3, 0.68 eV) can be found for a minimum threshold, demonstrating a 30% reduction compared to a bare microcavity. On the other hand, we can see that a 25% reduction of threshold can be achieved in a wide range of parameters, with $V_m > 10^4$ nm^3 and $\Delta_{ca} > 0.5$ eV, and the threshold reduction only excludes the region of small V_m and Δ_{ca}. It shows that the hybrid cavity provides a flexible and robust platform for realizing low-threshold nanolaser, without requiring the precise control of system parameters. As Eq. (19) indicates, the threshold is determined by the Purcell rate and the plasmon-induced QE decay, which we plot in Figs. 2(b) and 2(c), respectively. We can see that the small V_m and Δ_{ca} indeed produce larger C_{eff}, however, the enhancement of C_{eff} is much smaller than γ_m. For $V_m = 1.5 \times 10^4$ nm^3, γ_m manifests a threefold enhancement when Δ_{ca} decreases from 0.7 eV to 0.3 eV, while the enhancement of C_{eff} is less than 15% due to the great plasmon-induced dissipation of microcavity at small Δ_{ca}. Furthermore, as we discuss above, the threshold is linearly increased with γ_m. These two factors together make the small Δ_{ca} unsuitable for reducing the lasing threshold, and the same conclusion can be drawn for V_m.

Figures 2(d) and 2(e) show another configuration with a smaller mode volume of microcavity $V_c = 0.06 \mu$m^3, and thus stronger QE-cavity interaction. In this case, the minimum threshold achieves at smaller V_m and larger Δ_{ca}. A 37% reduction of lasing threshold is found, with the optimal parameters $(V_m, \Delta_{ca}) = (6 \times 10^3$ nm^3, 1.08 eV). The threshold curves shown in Fig. 2(f) imply that the hybrid cavity is suitable for QEs operating at near infrared, such as InAs/GaAs QDs [56,57] and InAs/InP QDs [58], and are thus promising in fabricating the room-temperature nanolaser operating at communication bands.

Figure 3(a) plots the normalized lasing threshold of a hybrid cavity as the function of Δ_{ca} and QE number N, for mode volumes $V_m = 1.5 \times 10^4$ nm^3 and $V_c = 0.15 \mu$m^3. The minimal QE number for lasing a hybrid cavity is $N_{\text{min}} = 21$, while the bare microcavity needs more than 30 QEs to lase. However, we can see that N reaches the minimum at $\Delta_{ca} = 0.4$ eV and becomes larger as Δ_{ca} increases. This phenomenon can be understood from Eq. (18), which indicates that the lasing requires the minimal QE number $N_{\text{min}} \approx$
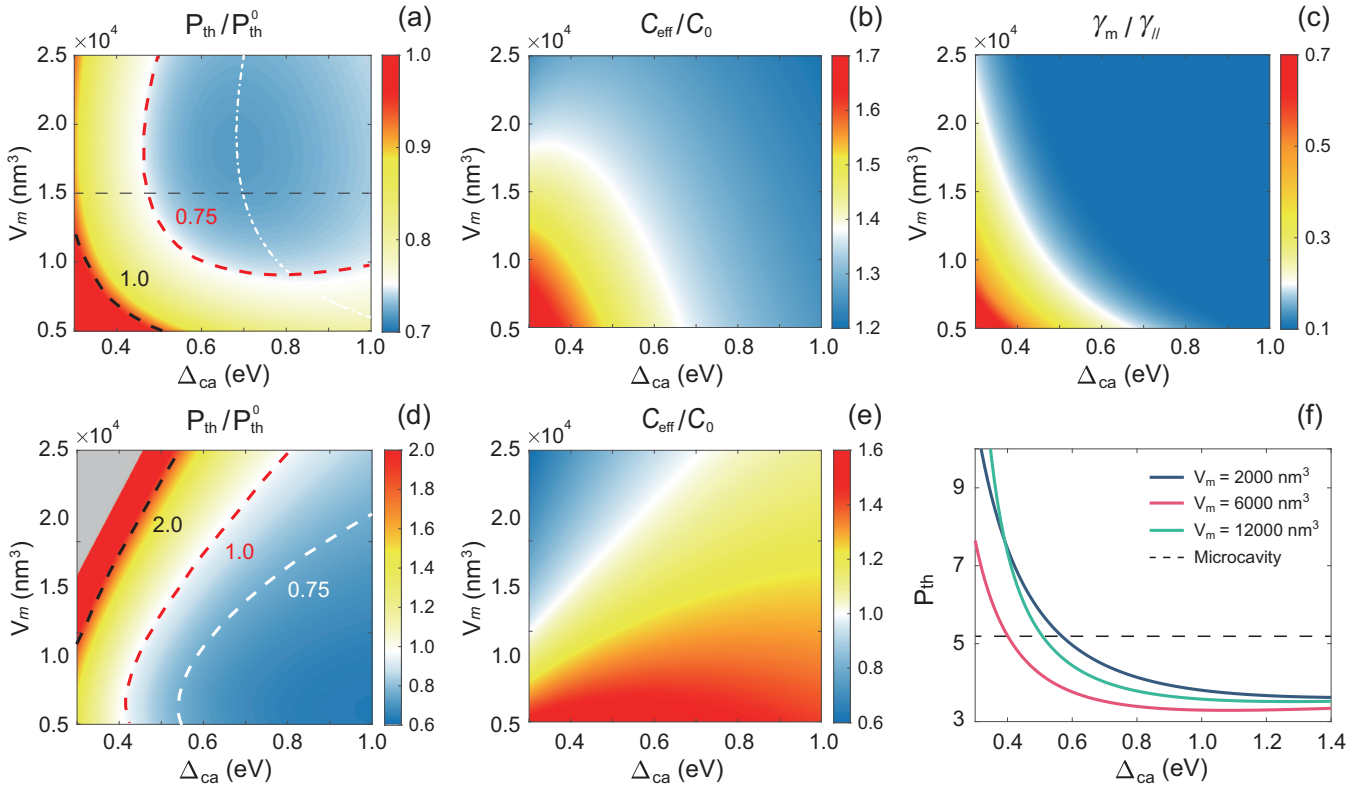
FIG. 2. (a)–(c) Contour plot of $P_{\text{th}}/P_{\text{th}}^0$, C_{eff}/C_0, and $\gamma_m/\gamma_{//}$ versus V_m and Δ_{ca}. The white dashed-dotted line traces the minimum P_{th}. (d) and (e) are the same as (a) and (b), respectively, but for $V_c = 0.06\,\mu\text{m}^3$ and $N = 15$. (f) Lasing threshold versus Δ_{ca} for various V_m. Other parameters are the same as (d).

$(2\gamma_p + \gamma_{//}P_{\text{th}})/4C_{\text{eff}}$. Since we assume a large γ_p, then $N_{\min}$ mainly depends on C_{eff}, which reaches the maximum at $\Delta_{ca} \approx$

FIG. 3. (a) Contour plot of $P_{\text{th}}/P_{\text{th}}^0$ as a function of N and Δ_{ca}. The white area is the parameter region where the lasing can occur in the hybrid cavity but not in the microcavity, while in the gray area both hybrid and microcavity cannot lase. The mode volumes are $V_m = 1.5 \times 10^4\,\text{nm}^3$ and $V_c = 0.15\,\mu\text{m}^3$. (b) is the same as (a) while $V_c = 0.06\,\mu\text{m}^3$. (c), (d) n_c and the corresponding linewidth $\Delta\nu$ as a function of incoherent pump rate for $N = 20$ and $V_m = 6 \times 10^3\,\text{nm}^3$. Other parameters are the same as (b).

0.35 eV, as Fig. 2(b) shows. The increasing of the QE number rapidly decreases the threshold pump to the value that is comparable to γ_m, thus γ_m takes effect and the optimal Δ_{ca} corresponding to $N_{\min}$ becomes larger. For the microcavity with $V_c = 0.06\,\mu\text{m}^3$, stronger QE-cavity interaction lowers the requirement of the QE number to lase, and $N_{\min}$ for both kinds of cavities are close, as Fig. 3(b) shows. Even in this case, the hybrid cavity can demonstrate a significant reduction of lasing threshold with small N. Therefore, we can expect that the hybrid cavity has a prominent advantage in few-atom lasing; however, it requires QME [Eq. (4)] instead of the semiclassical MB equations to describe such a nanolaser.
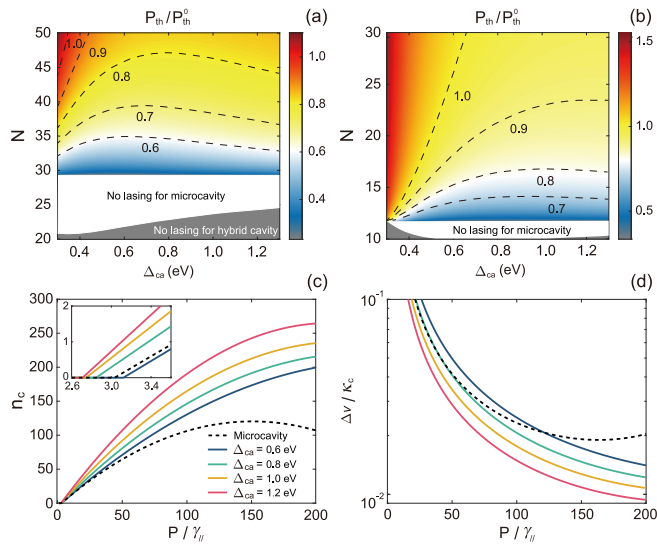
On the other hand, Figs. 3(a) and 3(b) show that a QE ensemble with large N seems to diminish or even reverse the positive effect of the introduced plasmonic antenna. Figure 3(c) compares the input-output curves of a bare microcavity and hybrid cavity with QE number $N = 20$. It shows that though the lasing threshold of the bare microcavity is lower than the hybrid cavity for $\Delta_{ca} = 0.6\,\text{eV}$, its field intensity demonstrates an early self-quenching around $P = 150\gamma_{//}$, where the averaged photon number is about 125 and much smaller than the maximum n_c of the hybrid cavity, which can reach ~200 for $\Delta_{ca} = 0.6\,\text{eV}$ and ~270 for $\Delta_{ca} = 1.2\,\text{eV}$.

Besides the threshold and field intensity, linewidth is another important quantity for characterizing lasing behavior. To evaluate the linewidth, we rewrite the atomic polarization and cavity field operators as the sum of a steady-state term X^s and a fluctuation term δX, i.e., $X = X^s + \delta X$ [59,60].

The linearization of Eqs. (10) and (11) yields the following equations for fluctuations:

$$\delta \dot{v}_- = -\frac{\gamma_{\text{eff}}}{2} \sec(\theta) e^{i\theta} \delta v_- + g e^{i\theta} \left(\langle \sigma_z^s \rangle \delta c + \delta \sigma_z \langle c^s \rangle \right) + F_{v_-} \tag{20}$$

$$\delta \dot{c} = -\frac{\kappa_{\text{eff}}}{2} \sec(\theta) e^{i\theta} \delta c + N g e^{i\theta} \delta v_-, \tag{21}$$

where $v_- = -i \langle \sigma_- \rangle$, and we introduced the Langevin noise operator for QE polarization F_{v_-}. The phase quadrature for field fluctuation, which is related to the linewidth of laser field, is expressed as $\delta \varphi = \text{Im}[\delta c - \delta c^*]/2i$. With $\theta \approx 0$, which is true for $|\Delta_{ca}| \gg |\Delta_{0c}|$, the fluctuation spectrum for phase quadrature of the cavity field can be obtained from Eqs. (20) and (21),

$$(\delta \varphi)_\omega = \frac{D_{v_+ v_-}}{2\omega^2} \frac{N^2 g^2 \cos(\theta)^2}{\omega^2 + (\kappa_{\text{eff}} + \gamma_{\text{eff}})^2/4}, \tag{22}$$

where we have used the correlation function $\langle F_{v_+}(\omega) F_{v_-}(\omega') \rangle = 2 D_{v_+ v_-} \delta(\omega + \omega')$, with the diffusion coefficient $2 D_{v_+ v_-} = \gamma_{\text{eff}} (\langle \sigma_z^s \rangle + 1)/2$, according to the fluctuation-dissipative theorem [40,61]. From Eq. (22), we can evaluate the low-frequency asymptotic of the spectral correlation function for phase quadrature component as $\langle \delta \varphi(\omega) \delta \varphi(\omega') \rangle = n_c \omega^{-2} \Delta v \delta(\omega + \omega')$ [62], where the linewidth Δv is given by

$$\Delta v = \frac{\kappa_c \kappa_{\text{eff}} \gamma_{\text{eff}}}{(\kappa_{\text{eff}} + \gamma_{\text{eff}})^2} \frac{\hbar \omega_c'}{P_{\text{out}}} N^2 \langle \sigma_{ee}^s \rangle C_{\text{eff}}, \tag{23}$$

where $P_{\text{out}} = \hbar \omega_c' \kappa_c n_c$ is the mean power of the laser field exciting the cavity and $\langle \sigma_{ee}^s \rangle = (\langle \sigma_z^s \rangle + 1)/2$.

In Fig. 3(d), we plot the linewidth of the laser field. We can see that even the hybrid cavity with $\Delta_{ca} = 0.8$ eV has a lower threshold and higher field intensity than a bare microcavity; it features comparable phase and intensity fluctuations for $P < 50 \gamma_{//}$, implying that the plasmonic antenna introduces extra dissipation to the system. However, the advantage of the hybrid cavity is obvious at high pump rate. For example, the linewidth of the hybrid cavity with $\Delta_{ca} = 0.6$ eV can be narrower than the bare microcavity when $P > 120 \gamma_{//}$; while for the hybrid cavity with $\Delta_{ca} = 1.2$ eV, a 50% narrowing of linewidth can be found at $P = 150 \gamma_{//}$.

In Fig. 4(a), we compare the self-quenching and the output power of laser field for a hybrid cavity and bare microcavity. For a configuration of a hybrid cavity with parameters $V_m = 1.5 \times 10^4$ nm^3, $V_c = 0.15$ μm^3, and $\Delta_{ca} = 0.7$ eV, a QE number $N = 40$ can sustain lasing output at $P = 350 \gamma_{//}$, while for a bare microcavity the lasing action terminates at $P = 180 \gamma_{//}$. Furthermore, we can see that even the enhancement of lasing output power of the hybrid cavity drops as N increases [see η plotted in the right of Fig. 4(a)], the difference of termination pump rate enlarges.

In the end of this section, we address an important issue: to what extent the lasing threshold can be reduced by using a hybrid cavity. Figure 4(b) plots the minimum of the normalized threshold as the function of $|g_1|$ and g_a instead of mode volumes, which is beneficial to explore the limit of threshold reduction. It shows that the strong plasmon-photon interaction is favorable and a coupling strength of
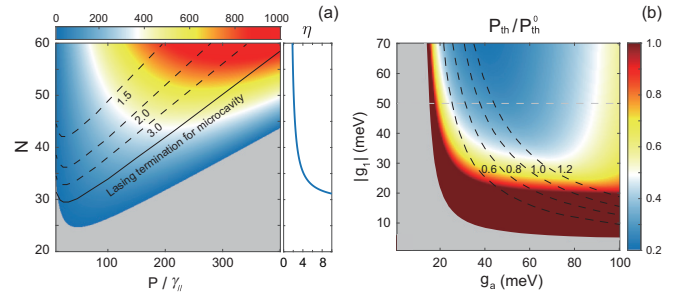

FIG. 4. (a) Contour plot of n_c of hybrid cavity versus N and P. The parameters are $V_m = 1.5 \times 10^4$ nm^3, $V_c = 0.15$ μm^3, and $\Delta_{ca} = 0.7$ eV. The dashed lines denote the ratio of n_c of hybrid cavity to that of microcavity. The solid black line plots the boundary where the lasing terminates in microcavity, while the gray area indicates the lasing termination in hybrid cavity. $\eta = \max[n_c]/\max[n_c^0]$ is the enhancement of the maximum lasing output for hybrid cavity, where n_c^0 is the steady-state photon number of bare microcavity. (b) Contour plot of the minimum $P_{\text{th}}/P_{\text{th}}^0$ as the function of the coupling strengths of g_1 and g_a for $N = 10$ and $g_c = 0.54$ meV. The dashed lines indicate the corresponding plasmon-photon detuning $\Delta_{ca} = 0.6, 0.8, 1.0$ and 1.2 eV.

$|g_1| > 20$ meV is required for reducing the threshold. This value is easily achieved for nanophotonic structures like the dimer rod-on-nanobeam [27,52]. Figure 4(b) also shows that with $|g_1| = 40$ meV and moderate QE-plasmon coupling strength ($g_a \approx 50$ meV), more than 50% reduction of the lasing threshold is achievable. A 70% reduction of threshold can also be found with $|g_1| = 70$ meV; however, a coupling strength exceeding 50 meV is hard to achieve for plasmon-photon interaction, which may require elaborate design of a hybrid cavity [52,54].

IV. A PHYSICAL REALIZATION

We now go beyond the prototype model and demonstrate the lasing threshold reduction in a realistic hybrid cavity. Figure 5(a) depicts the structure and the geometry parameters of the hybrid cavity, which is based on a SiN WGM microdisk resonator, with a plasmonic antenna on the top of the microdisk. For a QE oriented at the radial direction of the microdisk and located in the gap center of the antenna, Fig. 5(b) shows the Purcell factor $P(\omega)$ obtained from EM simulations in the frequency range of 1.4 eV to 1.7 eV, where the hybrid cavity manifests about 20 times enhancement of the Purcell effect compared to a bare microcavity. The spectral density connects with the Purcell factor through relation $P(\omega) = 2\pi J(\omega)/\gamma_{//} + 1$. Figures 5(c) and 5(d) compare the spectral density around two cavity resonances $\omega_c = 1.5670$ eV and 1.5151 eV, respectively. The former corresponds to the WGM mode for the maximum Purcell factor of the hybrid cavity.

To investigate the lasing characteristics of the hybrid cavity, we need to determine the coupling strengths in modified MB equations. This can be done by fitting the spectral density of hybrid cavity using the analytical expressions Eqs. (14)–(16) derived from the two-mode cQED model. Taking the cavity resonance $\omega_c = 1.5670$ eV for an
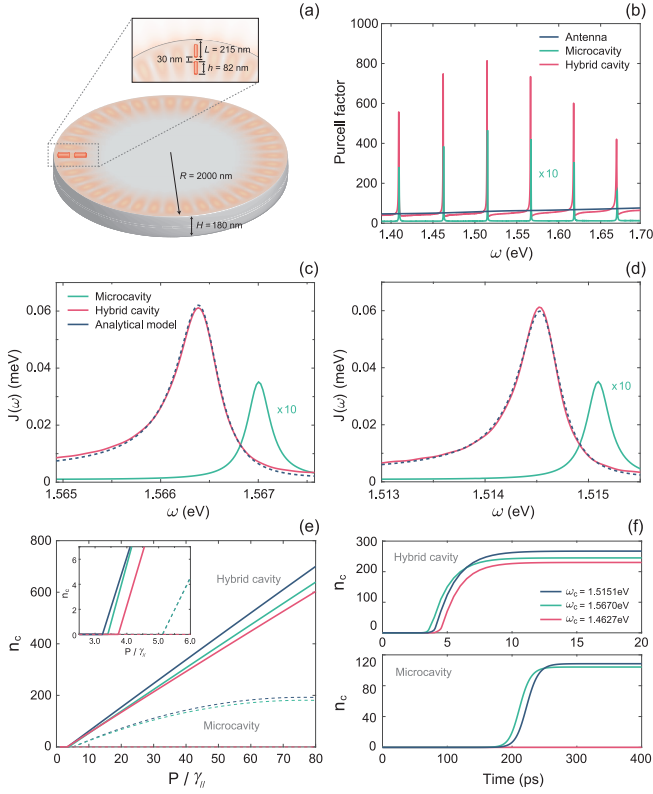
FIG. 5. (a) Schematic diagram of a hybrid cavity consisting of a WGM microcavity and a gold dimer rods. The gap of gold dimer is 30 nm, and the diameter of rods is 40 nm. Other geometry parameters are indicated in the figure. The refractive index of microcavity is $n = 2$, the permittivity also has an imaginary component of 4×10^{-6} to include the material absorption. (b) Purcell factor for plasmonic antenna, microcavity, and hybrid cavity. (c), (d) The fitting results of the spectral density of hybrid cavity for two cavity resonances, $\omega_c = 1.5670$ eV and 1.5151 eV, respectively. The fitting is based on the cQED model of the spectral density given by Eqs. (14)–(16). (e) n_c of hybrid cavity and microcavity as the function of pump rate P for $N = 100$. The inset compares n_c at the low pump. (f) shows the corresponding time evolution of n_c for hybrid cavity (upper panel) and microcavity (lower panel) at $P = 30\gamma_{//}$ in (e).

example, the parameters of bare components are evaluated as $(\kappa_c, g_c) = (0.2958 \text{ meV}, 29.33 \,\mu\text{eV})$ and $(\omega_a, \kappa_a, g_a) = (2.25 \text{ eV}, 255 \text{ meV}, 3.31 \text{ meV})$ for microcavity and plasmonic antenna, respectively. Subsequently, the plasmon-photon interaction is determined as $g_1 = -20.2$ meV by simple curve fitting using Eqs. (14)–(16). The black dashed lines in Figs. 5(c) and 5(d) show the analytical results, where we can see good accordance between the EM simulations and the cQED model. Note that for the WGM mode of $\omega_c = 1.5151$ eV [Fig. 5(d)], we obtain $(\kappa_c, g_c) = (0.3093 \text{ meV}, 30 \,\mu\text{eV})$, while other parameters remain the same as Fig. 5(c).

Figure 5(e) compares the input-output curves of a hybrid cavity and bare microcavity for various ω_c, where the WGM mode of $\omega_c = 1.4627$ eV cannot lase in a microcavity. The lasing threshold of a hybrid cavity exhibits a reduction of about 40% for the other two WGM modes. Furthermore, the lasing output of a hybrid cavity still linearly increases at

$P = 80\gamma_{//}$ with $n_c > 600$, while the bare microcavity reaches the maximum of $n_c \approx 200$. Figure 5(f) displays the time evolution of the laser field intensity, where the hybrid cavity starts to lase at 4 ps after applying the QE pump, and reaches the steady state within 6 ps. By contrast, the lasing action of bare microcavity onsets at around 200 ps, and takes 50 ps to reach the maximum. The results not only confirm the lasing threshold reduction of a hybrid cavity but also demonstrate the advantages in fast response and switching of lasing action due to the introduction of plasmonic antenna.

Finally, it is worth noting that the above results and conclusions are also valid for other configurations of hybrid cavities, for example, where the plasmonic antenna is inside the WGM resonator [42] or replaced by 2D transition metal dichalcogenide materials [63,64], since their spectral densities share similar features with the plasmonic-photonic cavity studied in this paper.

V. CONCLUSION

In conclusion, we propose a general method to reduce the lasing threshold of various microcavity-based nanolasers by coupling to an off-resonant plasmonic antenna, and develop the corresponding two-level nanolaser theory. We find that compared to a bare dielectric microcavity, a hybrid cavity with suitable plasmon-photon detuning can have prominent advantages in terms of lasing threshold, linewidth, output power, and switching time at a wide range of parameters. Our paper opens a pathway for realizing low-threshold and high-power nanolasers at ambient conditions.

APPENDIX A: DERIVATION OF THE MODIFIED MAXWELL-BLOCH EQUATIONS

The Hamiltonian of the system under the RWA is written as

$$H = H_0 + H_I, \tag{A1}$$

with

$$H_0 = \omega_a a^\dagger a + \omega_c c^\dagger c + \omega_0 \sum_k^N \sigma_+^k \sigma_-^k, \tag{A2}$$

$$H_I = \sum_k^N g_a^k (a^\dagger \sigma_-^k + \sigma_+^k a) + \sum_k^N g_c^k (c^\dagger \sigma_-^k + \sigma_+^k c) + g_1 (a^\dagger c + a c^\dagger). \tag{A3}$$

The expectation value of operator O is given by $\langle \dot{O} \rangle =$ $\text{Tr}[iO[\rho, H] + O\mathcal{L}_{L_i}(\rho)]$, where ρ is the density matrix and the Lindblad superoperators $\mathcal{L}_{L_i}(\rho)$ takes the form

$$\mathcal{L}_{L_i}(\rho) = \frac{1}{2}\left(2L_i\rho L_i^\dagger - \{L_i^\dagger L_i, \rho\}\right) \tag{A4}$$

with $L_1 = \sqrt{P\gamma_{//}}\sigma_+$ for QE pump, $L_2 = \sqrt{\gamma_{//}}\sigma_-$ for QE SE, $L_3 = \sqrt{\gamma_p}\sigma_z$ for QE dephasing, $L_4 = \sqrt{\kappa_a}a$ for plasmonic decay, and $L_5 = \sqrt{\kappa_c}c$ for microcavity decay. We thus can obtain the following equations of motion:

$$\dot{a} = -i\left(\omega_a - i\frac{\kappa_a}{2}\right)a - i\sum_k^N g_a^k\sigma_-^k - ig_1c, \tag{A5}$$

$$\dot{c} = -i\left(\omega_c - i\frac{\kappa_c}{2}\right)c - i\sum_k^N g_c^k\sigma_-^k - ig_1a, \tag{A6}$$

$$\dot{\sigma}_-^k = -i\left(\omega_0 - i\frac{\gamma_\perp}{2}\right)\sigma_-^k + ig_a^k\sigma_z^k a + ig_c^k\sigma_z^k c, \tag{A7}$$

$$\dot{\sigma}_z^k = 2ig_a^k\left(a^\dagger\sigma_-^k - \sigma_+^k a\right) + 2ig_c^k\left(c^\dagger\sigma_-^k - \sigma_+^k c\right) - \gamma_{//}\left(\sigma_z^k + 1\right) + \gamma_{//}P\left(1 - \sigma_z^k\right), \tag{A8}$$

where we have neglected the QE-field correlation by factorizing the second-order expectation values $\langle\sigma_z^k c\rangle$, $\langle c^\dagger\sigma_-^k\rangle$ and $\langle\sigma_+^k c\rangle$ into the products of the first-order expectation values $\langle\sigma_z^k\rangle\langle c\rangle$, $\langle c^\dagger\rangle\langle\sigma_-^k\rangle$, and $\langle\sigma_+^k\rangle\langle c\rangle$, respectively. We also omit the angle brackets $\langle\cdot\rangle$ that indicate the expectation values in

Eqs. (A5)–(A8). The formal integration of Eqs. (A5)–(A7) yields

$$a(t) = a(t_0)e^{-i(\omega_a - i\frac{\kappa_a}{2})t} - i\int_{t_0}^t \left(\sum_k^N g_a^k\sigma_-^k(\tau) + g_1c(\tau)\right)e^{-i(\omega_a - i\frac{\kappa_a}{2})(t-\tau)}d\tau, \tag{A9}$$

$$c(t) = c(t_0)e^{-i(\omega_c - i\frac{\kappa_c}{2})t} - i\int_{t_0}^t \left(\sum_k^N g_c^k\sigma_-^k(\tau) + g_1a(\tau)\right)e^{-i(\omega_c - i\frac{\kappa_c}{2})(t-\tau)}d\tau, \tag{A10}$$

$$\sigma_-^k(t) = \sigma_-^k(t_0)e^{-i(\omega_0 - i\frac{\gamma_\perp}{2})t} + i\int_{t_0}^t \left(g_a^k\sigma_z^k(\tau)a(\tau) + g_c^k\sigma_z^k(\tau)c(\tau)\right) \times e^{-i(\omega_0 - i\frac{\gamma_\perp}{2})(t-\tau)}d\tau. \tag{A11}$$

The photonic mode and QEs dynamics are less affected by plasmonic antennas for large plasmonic-photonic detuning, and thus we can apply the Markovian approximation to obtain

$$c(\tau) = c(t)e^{i(\omega_c - i\frac{\kappa_c}{2})(t-\tau)}, \tag{A12}$$

$$\sigma_-^k(\tau) = \sigma_-^k(t)e^{i(\omega_0 - i\frac{\gamma_\perp}{2})(t-\tau)}. \tag{A13}$$

Substituting back into Eq. (A9), we have

$$a(t) = a(t_0)e^{-i(\omega_a - i\frac{\kappa_a}{2})t} - i\int_{t_0}^t \sum_k^N g_a^k\sigma_-^k(t)e^{i(\omega_0 - i\frac{\gamma_\perp}{2})(t-\tau)}e^{-i(\omega_a - i\frac{\kappa_a}{2})(t-\tau)}d\tau\ i\int_{t_0}^t g_1c(t)e^{i(\omega_c - i\frac{\kappa_c}{2})(t-\tau)}e^{-i(\omega_a - i\frac{\kappa_a}{2})(t-\tau)}d\tau,$$

$$= a(t_0)e^{-i(\omega_a - i\frac{\kappa_a}{2})t} - i\int_{t_0}^t \sum_k^N g_a^k\sigma_-^k(t)e^{-i((\omega_a - \omega_0) - i\frac{(\kappa_a - \gamma_\perp)}{2})(t-\tau)}d\tau - i\int_{t_0}^t g_1c(t)e^{-i((\omega_a - \omega_c) - i\frac{(\kappa_a - \kappa_c)}{2})(t-\tau)}d\tau. \tag{A14}$$

By changing the integration variable τ to $t' = t - \tau$, we can obtain

$$a(t) = a(t_0)e^{-i(\omega_a - i\frac{\kappa_a}{2})t} - i\int_0^{t-t_0} \sum_k^N g_a^k\sigma_-^k(t)e^{-i((\omega_a - \omega_0) - i\frac{(\kappa_a - \gamma_\perp)}{2})t'}dt' - i\int_0^{t-t_0} g_1c(t)e^{-i((\omega_a - \omega_c) - i\frac{(\kappa_a - \kappa_c)}{2})t'}dt'. \tag{A15}$$

Omitting the fast decay terms, we obtain

$$a(t) \approx -\frac{\sum_k^N g_a^k\sigma_-^k(t)}{(\omega_a - \omega_0) - i\frac{(\kappa_a - \gamma_\perp)}{2}} - \frac{g_1c(t)}{(\omega_a - \omega_c) - i\frac{(\kappa_a - \kappa_c)}{2}}. \tag{A16}$$

Plugging Eq. (A16) back into Eqs. (A6)–(A8), we arrive at the modified MB equations Eqs. (10)–(12) in the main text,

$$\dot{\sigma}_-^k = -i\left(\omega_0^{k'} - i\frac{\gamma_{eff}^k}{2}\right)\sigma_-^k + ig_{eff}^k\sigma_z^k c, \tag{A17}$$

$$\dot{c} = -i\left(\omega_c' - i\frac{\kappa_{eff}}{2}\right)c - i\sum_k g_{eff}^k\sigma_-^k, \tag{A18}$$

$$\dot{\sigma}_z^k = 2i\left(g_{eff}^{k*}c^\dagger\sigma_-^k - g_{eff}^k\sigma_+^k c\right) - \left(\gamma_{//} + \gamma_m^k\right)\left(\sigma_z^k + 1\right) + \gamma_{//}P\left(1 - \sigma_z^k\right). \tag{A19}$$

APPENDIX B: LASING CHARACTERISTICS

If the transition frequency of the QE does not match the resonance frequency of the lasing mode, the lasing frequency is not equal to either of them. We can see that Eqs. (A18) and (A19) always have a trivial zero solution, while the nontrivial solution corresponds to the lasing action, which can be found from the characteristic matrix of Eqs. (A18) and (A19) [43],

$$\begin{pmatrix} \omega_c' + \Delta_{c0} - i\frac{\gamma_{eff}}{2} - \omega_s & -ge^{i\theta}\sigma_z^s \\ Nge^{i\theta} & \omega_c' - i\frac{\kappa_{eff}}{2} - \omega_s \end{pmatrix}, \tag{B1}$$

where ω_s is the lasing frequency and Δ_{c0} stands for the frequency detuning between the QE and the lasing mode.

We made the assumption of an identical QE and let $g_{\mathrm{eff}} \equiv g e^{i\theta}$. By separating the real and imaginary parts of

the determinant of Eq. (B1) and setting to be zero, we have

$$\omega_s^2 - (\Delta_{c0} + 2\omega_c')\omega_s + \omega_c'^2 + \Delta_{c0}\omega_c' - \frac{\kappa_{\mathrm{eff}}\gamma_{\mathrm{eff}}}{4} + \sigma_z^s g^2 N \cos(2\theta) = 0, \tag{B2}$$

$$\omega_s(\kappa_{\mathrm{eff}} + \gamma_{\mathrm{eff}}) - (\kappa_{\mathrm{eff}} + \gamma_{\mathrm{eff}})\omega_c' - \kappa_{\mathrm{eff}}\Delta_{c0} + \sigma_e^s g^2 N \sin(2\theta) = 0. \tag{B3}$$

The solutions of Eqs. (B2) and (B3) with $\sigma_z^S > 0$ are

$$\omega_s = \omega_c' + \frac{\Delta_{c0} + (\kappa_{\mathrm{eff}} + \gamma_{\mathrm{eff}})\cot(2\theta) - \sqrt{[\Delta_{c0} + (\kappa_{\mathrm{eff}} + \gamma_{\mathrm{eff}})\cot(2\theta)]^2 + 4\kappa_{\mathrm{eff}}[\gamma_{\mathrm{eff}} - \Delta_{c0}\cot(2\theta)]}}{2}, \tag{B4}$$

$$\sigma_z^s = \frac{\csc(2\theta)}{2g^2 N}\left(\Delta_{c0}(\kappa_{\mathrm{eff}} - \gamma_{\mathrm{eff}}) - (\kappa_{\mathrm{eff}} + \gamma_{\mathrm{eff}})^2 \cot(2\theta)\right)$$

$$+ \frac{(\kappa_{\mathrm{eff}} + \gamma_{\mathrm{eff}})\sqrt{\Delta_{c0}^2 + \kappa_{\mathrm{eff}}^2 + \gamma_{\mathrm{eff}}^2 + 6\kappa_{\mathrm{eff}}\gamma_{\mathrm{eff}} + \left[(\kappa_{\mathrm{eff}} - \gamma_{\mathrm{eff}})^2 - \Delta_{c0}^2\right]\cos(2\theta) - 2\Delta_{c0}(\kappa_{\mathrm{eff}} - \gamma_{\mathrm{eff}})\sin(2\theta)}}{2\sqrt{2}g^2 N \sin(2\theta)^2}. \tag{B5}$$

We find the optimal Δ_{c0} for the minimal lasing threshold by solving $\partial\sigma_z^s / \partial\Delta_{c0} = 0$, and the result is $\Delta_{c0} = (\gamma_{\mathrm{eff}} - \kappa_{\mathrm{eff}})\tan(\theta)/2$. Substituting back into Eqs. (B4) and (B5), we can obtain the steady-state population inversion $\sigma_z^S = \kappa_{\mathrm{eff}}\gamma_{\mathrm{eff}}/4Ng^2\cos^2(\theta)$ and the corresponding lasing frequency $\omega_s = \omega_c' - \kappa_{\mathrm{eff}}\tan(\theta)/2$.

APPENDIX C: ANALYTICAL EXPRESSIONS OF THE SPECTRAL DENSITY OF HYBRID CAVITY

The hybrid cavity constructs a structured environment that features a non-Lorentzian spectral density, which in general requires to be treated as continuous bosonic modes in cQED [65,66]. By decomposing the system in a non-Markovian core (QE cavities and cavity-cavity interaction) and Markovian environment (cavity-reservoir interaction), the Hamiltonian of the hybrid cavity reads

$$H' = H_0' + H_I', \tag{C1}$$

with the free Hamiltonian H_0' and interaction Hamiltonian H_I',

$$H_0' = \omega_a a^\dagger a + \omega_c c^\dagger c + \sum_\mu \omega_\mu \alpha_\mu^\dagger \alpha_\mu, \tag{C2}$$

$$H_I' = \sum_\mu \left[(V_\mu a^\dagger + U_\mu c^\dagger)\alpha_\mu + \alpha_\mu^\dagger(V_\mu^* a + U_\mu^* c)\right] + g_1(a^\dagger c + c^\dagger a), \tag{C3}$$

where the Markovian environment is described by a bosonic reservoir, with α_μ and ω_μ being the annihilation operator and frequency of the μth mode, respectively. V_μ and U_μ are the corresponding coupling strengths to plasmonic antenna and microcavity, respectively. We can obtain the equations of motion for three bosonic fields:

$$\dot{a} = -i\omega_a a - ig_1 c - i\sum_\mu V_\mu \alpha_\mu, \tag{C4}$$

$$\dot{c} = -i\omega_c c - ig_1 a - i\sum_\mu U_\mu \alpha_\mu, \tag{C5}$$

$$\dot{\alpha}_\mu = -i\omega_\mu \alpha_\mu - i(V_\mu^* a + U_\mu^* c). \tag{C6}$$

Formally integrating the equation for α_μ, we have

$$a_\mu = e^{-i\omega_\mu(t-t_0)}\alpha_\mu^0 - i\int_0^t d\tau e^{-i\omega_\mu(t-\tau)}(V_\mu^* a + U_\mu^* c), \tag{C7}$$

where a_μ^0 stands for the initial conditions at $t = 0$. The cavity-reservoir interaction follows the Markovian dynamics, thus it is sufficient to use the zero-order approximation $a(\tau) \approx a(t)e^{i\omega_a(t-\tau)}$ and $c(\tau) \approx c(t)e^{i\omega_c(t-\tau)}$. Substituting into Eq. (C7), we obtain

$$a_\mu = -i\int_0^t d\tau e^{i(\omega_\mu - \omega_a)(\tau - t)}V_\mu^* a - i\int_0^t d\tau e^{i(\omega_\mu - \omega_c)(\tau - t)}U_\mu^* c, \tag{C8}$$

where we assume the initial condition $a_\mu^0 = 0$. The time integration yields a delta function and thus

$$a_\mu = -i\pi\delta(\omega_\mu - \omega_a)V_\mu^* a - i\pi\delta(\omega_\mu - \omega_c)U_\mu^* c. \tag{C9}$$

Plugging back into Eqs. (C4) and (C5), we arrive at

$$\dot{a} = -i\left(\omega_a - \frac{i\kappa_a}{2}\right)a - i\left(g_1 - i\frac{\sqrt{\kappa_a^0\kappa_c}}{2}\right)c, \tag{C10}$$

$$\dot{c} = -i\left(\omega_c - \frac{i\kappa_c}{2}\right)c - i\left(g_1 - i\frac{\sqrt{\kappa_a^0\kappa_c}}{2}\right)a, \tag{C11}$$

where $\kappa_a^0 = 2\pi|V|^2$, $\kappa_c^0 = 2\pi|U|^2$ and we assume the response of reservoir is flat enough compared to the linewidth of cavities so V and U are frequency independent and the subscript μ has been dropped. Note that κ_a^0 represents the radiative cavity decay. The typical value of κ_a^0 for plasmonic antenna is $\sim 10\,\mathrm{meV}$, and thus we can assume a real coupling strength between two cavities. The spectral density of hybrid cavity is given by [38,65,66]

$$J(\omega) = \int_{-\infty}^{+\infty} d\tau \langle[g_a a(\tau) + g_c c(\tau)][g_a a^\dagger(0) + g_c c^\dagger(0)]\rangle e^{i\omega\tau}, \tag{C12}$$

where the two-time correlation functions $\langle a(\tau)a^\dagger(0)\rangle$, $\langle a(\tau)c^\dagger(0)\rangle$, and $\langle c(\tau)c^\dagger(0)\rangle$ can be calculated using the quantum regression theorem with Eqs. (C10) and (C11). Then we can obtain the analytical expression of the spectral density of a hybrid cavity using the independent parameters of two cavities

and their coupling strength, which is given by

$$J(\omega) = -g_c^2 \, \text{Im} \, [J_c(\omega)] - 2g_a g_c \, \text{Im} \, [J_{ac}(\omega)] - g_a^2 \, \text{Im} \, [J_a(\omega)],$$

(C13)

with

$$J_X(\omega) = \chi_X(\omega) \big[1 - g_1^2 \chi_a(\omega) \chi_c(\omega)\big]^{-1},$$

(C14)

$$J_{ac}(\omega) = g_1 \chi_a(\omega) \chi_c(\omega) \big[1 - g_1^2 \chi_a(\omega) \chi_c(\omega)\big]^{-1},$$

(C15)

where $\chi_X(\omega) = [(\omega - \omega_X) + i\kappa_X/2]^{-1}$ for $X = a, c$. In Fig. 1(c) in the main text, the spectral density plotted with dashed lines are given by Eqs. (C13)–(C15).

For large plasmonic-photonic detuning, we can replace $\chi_a(\omega)$ by $\chi_a(\omega_a)$ in Eq. (C13). Then we can obtain the approximate expressions of three terms on the right-hand side of Eq. (C13), which allows us to find the maximal spectral density around the cavity frequency ω_c'. The first term is the plasmon-modified cavity response:

$$- \text{Im} \, [J_c(\omega)] = \frac{\frac{\kappa_{\text{eff}}}{2}}{(\omega - \omega_c')^2 + \left(\frac{\kappa_{\text{eff}}}{2}\right)^2}.$$

(C16)

We can see that this term shows a standard Lorentzian line shape with slight frequency shifting and broaden linewidth. The second term stands for the interference of two cavities:

$$- \text{Im} \, [J_{ac}(\omega)] = \frac{1}{g_1} \frac{\frac{\kappa_m}{2}(\omega - \omega_c') + \delta\omega_c \frac{\kappa_{\text{eff}}}{2}}{(\omega - \omega_c')^2 + \left(\frac{\kappa_{\text{eff}}}{2}\right)^2}.$$

(C17)

For nanolasers $2\delta\omega_c \gg \kappa_m$, the maximum approximately achieves at $\omega = \omega_c'$, and the corresponding linewidth is κ_{eff}. The last term is the cavity-modified antenna response, which presents a Fano line shape,

$$- \text{Im} \, [J_a(\omega)] = \frac{\kappa_m}{2g_1^2} \frac{(\Omega + q)^2 + \frac{C_1}{(1+r_c)^2}}{\Omega^2 + 1},$$

(C18)

where $\Omega = 2(\omega - \omega_c')/\kappa_{\text{eff}}$, $r_C = \kappa_m/\kappa_c$, $q = 2\delta\omega_c/\kappa_{\text{eff}}$, and $C_1 = 4g_1^2/\kappa_a\kappa_c$. For $C_1 \gg |q| > 1$, the linewidth is $\sim\kappa_{\text{eff}}$ and the maximum is located at ω_c'. Then the total spectral density at ω_c' is given by

$$J(\omega_c') = \frac{2}{\kappa_{\text{eff}}} \left(g_c^2 + \frac{2g_a g_c \delta\omega_c}{g_1} + g_a^2 \frac{\kappa_m \kappa_c}{\kappa_a \kappa_{\text{eff}}} \right).$$

(C19)

One can verify that if $\kappa_{\text{eff}} \approx \kappa_c$, then $J(\omega_c') = 2|g_{\text{eff}}|^2/\kappa_{\text{eff}}$, therefore around the cavity frequency ω_c' the spectral density $J(\omega)$ fits well with the effective model $J_{\text{eff}}(\omega) = |g_{\text{eff}}|^2 \frac{\kappa_{\text{eff}}/2}{(\omega - \omega_c')^2 + (\kappa_{\text{eff}}/2)^2}$, as Fig. 1(c) shows. The equivalence of two methods lies in the fact that the spectral density of a hybrid cavity with large plasmonic-photonic detuning presents a nearly perfect Lorentzian line shape around the resonance frequency of the photonic mode. Therefore, the modified MB equation is consistent with the quantum description of spectral density. The consistence breaks down in the case of small plasmonic-photonic detuning, where the plasmonic

mode strongly affects the dynamics of microcavity and QEs, and the spectral density evolves into a Fano shape.

APPENDIX D: EVALUATION OF COUPLING STRENGTHS FROM MODE VOLUMES

The coupling strength between the QEs and the photonic mode is given by

$$g_c = \mathbf{d} \cdot \mathbf{E_c},$$

(D1)

with cavity field

$$\mathbf{E_c} = \sqrt{\frac{\hbar\omega_c}{2\epsilon_0 V_c}} \mathbf{f}(\mathbf{r_0})(c^\dagger + c),$$

(D2)

where $\mathbf{f}(\mathbf{r_0})$ is the normalized electric field at QE position $\mathbf{r_0}$, and ϵ_0 is the permittivity of vacuum.

For a metallic nanoparticle, the electric field of a dipolar plasmonic mode interacting with an x-oriented dipole emitter (transversa plasmon-QE coupling) reads

$$\mathbf{E_a} = \sqrt{\frac{\hbar\omega_a}{2\epsilon_0 \epsilon_g V_m}} \mathbf{G}(\mathbf{r_0})(a^\dagger + a),$$

(D3)

where $\epsilon_g = \text{Re}\big[\frac{\partial(\omega\epsilon_m)}{\partial\omega}\big|_{\omega=\omega_a}\big]$, with ϵ_m being the metal permittivity. The mode distribution $\mathbf{G}(\mathbf{r})$ is given by [55,67]

$$\mathbf{G}(\mathbf{r}) = \begin{cases} \mathbf{n_x} & r < R \\ -\frac{R^3}{r^3}[3(\mathbf{n_x} \cdot \mathbf{n_r})\mathbf{n_r} - \mathbf{n_r}] & r > R, \end{cases}$$

(D4)

where $\mathbf{n_x}/\mathbf{n_r}$ is the unitary vector along $\mathbf{r}/\mathbf{x}$ direction and R is the radius of nanoparticle. The mode volume of plasmonic mode in Eq. (D3) can be evaluated as [55]

$$\begin{aligned} V_m &= \frac{\int_0^R |\mathbf{G}(\mathbf{r})|^2 \epsilon_g d^3\mathbf{r} + \int_R^\infty |\mathbf{G}(\mathbf{r})|^2 \epsilon_b d^3\mathbf{r}}{|\mathbf{G}(0)|^2 \epsilon_g} \\ &= \frac{4}{3}\pi R^3 \frac{2\epsilon_b + 1}{\epsilon_b + 1}, \end{aligned}$$

(D5)

where ϵ_b is the background permittivity. Then the coupling strength between the QEs and the plasmonic mode is straightforward,

$$g_a = \mathbf{d} \cdot \mathbf{E_a} = \mu \sqrt{\frac{\hbar\omega_a}{2\epsilon_0 \epsilon_g V_m}} \frac{R^3}{r^3},$$

(D6)

and the coupling strength of plasmonic-photonic interaction can be calculated as

$$g_1 = -2\pi R^3 \hbar \sqrt{\frac{\omega_1 \omega_c}{\epsilon_g V_m V_c}} |\mathbf{f}(\mathbf{r_a})|,$$

(D7)

where $\mathbf{r_a}$ is the location of nanoparticle. We assume $|\mathbf{f}(\mathbf{r_a})| = 1$ in calculations, and replace the physical radius R of nanoparticle by its mode volume in Eqs. (D6) and (D7) using Eq. (D5), so all coupling strengths can be determined through mode volumes.

[1] L. Liu, R. Kumar, K. Huybrechts, T. Spuesens, G. Roelkens, E.-J. Geluk, T. de Vries, P. Regreny, D. Van Thourhout, R. Baets, and G. Morthier, An ultra-small, low-power, all-optical flip-flop memory on a silicon chip, Nat. Photonics **4**, 182 (2010).

[2] V. Dolores-Calzadilla, B. Romeira, F. Pagliano, S. Birindelli, A. Higuera-Rodriguez, P. J. van Veldhoven, M. K. Smit, A. Fiore, and D. Heiss, Waveguide-coupled nanopillar metal-cavity light-emitting diodes on silicon, Nat. Commun. **8**, 14323 (2017).

[3] R.-M. Ma, X. Yin, R. F. Oulton, V. J. Sorger, and X. Zhang, Multiplexed and electrically modulated plasmon laser circuit, Nano Lett. **12**, 5396 (2012).

[4] S. Cho, M. Humar, N. Martino, and S. H. Yun, Laser Particle Stimulated Emission Microscopy, Phys. Rev. Lett. **117**, 193902 (2016).

[5] X. Liu, C. Kuang, X. Hao, C. Pang, P. Xu, H. Li, Y. Liu, C. Yu, Y. Xu, D. Nan, W. Shen, Y. Fang, L. He, X. Liu, and Q. Yang, Fluorescent Nanowire Ring Illumination for Wide-Field Far-Field Subdiffraction Imaging, Phys. Rev. Lett. **118**, 076101 (2017).

[6] E. I. Galanzha, R. Weingold, D. A. Nedosekin, M. Sarimollaoglu, J. Nolan, W. Harrington, A. S. Kuchyanov, R. G. Parkhomenko, F. Watanabe, Z. Nima, A. S. Biris, A. I. Plekhanov, M. I. Stockman, and V. P. Zharov, Spaser as a biological probe, Nat. Commun. **8**, 15528 (2017).

[7] P. Song, J.-H. Wang, M. Zhang, F. Yang, H.-J. Lu, B. Kang, J.-J. Xu, and H.-Y. Chen, Three-level spaser for next-generation luminescent nanoprobe, Sci. Adv. **4**, eaat0292 (2018).

[8] S. L. McCall, A. F. J. Levi, R. E. Slusher, S. J. Pearton, and R. A. Logan, Whispering-gallery mode microdisk lasers, Appl. Phys. Lett. **60**, 289 (1992).

[9] O. Painter, R. K. Lee, A. Scherer, A. Yariv, J. D. O'Brien, P. D. Dapkus, and I. Kim, Two-dimensional photonic band-gap defect mode laser, Science **284**, 1819 (1999).

[10] A. C. Tamboli, E. D. Haberer, R. Sharma, K. H. Lee, S. Nakamura, and E. L. Hu, Room-temperature continuous-wave lasing in GaN/InGaN microdisks, Nat. Photonics **1**, 61 (2007).

[11] I. Prieto, J. M. Llorens, L. E. Muñoz-Camúñez, A. G. Taboada, J. Canet-Ferrer, J. M. Ripalda, C. Robles, G. Muñoz-Matutano, J. P. Martínez-Pastor, and P. A. Postigo, Near thresholdless laser operation at room temperature, Optica **2**, 66 (2015).

[12] Y. Ota, M. Kakuda, K. Watanabe, S. Iwamoto, and Y. Arakawa, Thresholdless quantum dot nanolaser, Opt. Express **25**, 19981 (2017).

[13] A. Kodigala, T. Lepetit, Q. Gu, B. Bahari, Y. Fainman, and B. Kanté, Lasing action from photonic bound states in continuum, Nature (London) **541**, 196 (2017).

[14] S. T. Ha, Y. H. Fu, N. K. Emani, Z. Pan, R. M. Bakker, R. Paniagua-Domínguez, and A. I. Kuznetsov, Directional lasing in resonant semiconductor nanoantenna arrays, Nat. Nanotechnol. **13**, 1042 (2018).

[15] Z. Liu, J. Wang, B. Chen, Y. Wei, W. Liu, and J. Liu, Giant enhancement of continuous wave second harmonic generation from few-layer GaSe coupled to high-q quasi bound states in the continuum, Nano Lett. **21**, 7405 (2021).

[16] P. R. Rice and H. J. Carmichael, Photon statistics of a cavity-qed laser: A comment on the laserphase-transition analogy, Phys. Rev. A **50**, 4318 (1994).

[17] D. J. Bergman and M. I. Stockman, Surface Plasmon Amplification by Stimulated Emission of Radiation: Quantum Generation of Coherent Surface Plasmons in Nanosystems, Phys. Rev. Lett. **90**, 027402 (2003).

[18] M. A. Noginov, G. Zhu, A. M. Belgrave, R. Bakker, V. M. Shalaev, E. E. Narimanov, S. Stout, E. Herz, T. Suteewong, and U. Wiesner, Demonstration of a spaser-based nanolaser, Nature (London) **460**, 1110 (2009).

[19] M. I. Stockman, The spaser as a nanoscale quantum generator and ultrafast amplifier, J. Opt. **12**, 024004 (2010).

[20] G. Kewes, K. Herrmann, R. Rodriguez-Oliveros, A. Kuhlicke, O. Benson, and K. Busch, Limitations of Particle-Based Spasers, Phys. Rev. Lett. **118**, 237402 (2017).

[21] R.-M. Ma and R. F. Oulton, Applications of nanolasers, Nat. Nanotechnol. **14**, 12 (2019).

[22] J. B. Khurgin and G. Sun, Comparative analysis of spasers, vertical-cavity surface-emitting lasers and surface-plasmon-emitting diodes, Nat. Photonics **8**, 468 (2014).

[23] A. Delga, J. Feist, J. Bravo-Abad, and F. J. Garcia-Vidal, Quantum Emitters Near a Metal Nanoparticle: Strong Coupling and Quenching, Phys. Rev. Lett. **112**, 253601 (2014).

[24] V. N. Pustovit, A. M. Urbas, A. V. Chipouline, and T. V. Shahbazyan, Coulomb and quenching effects in small nanoparticle-based spasers, Phys. Rev. B **93**, 165432 (2016).

[25] L. S. Petrosyan and T. V. Shahbazyan, Spaser quenching by off-resonant plasmon modes, Phys. Rev. B **96**, 075423 (2017).

[26] H. M. Doeleman, E. Verhagen, and A. F. Koenderink, Antennacavity hybrids: Matching polar opposites for Purcell enhancements at any linewidth, ACS Photonics **3**, 1943 (2016).

[27] M. Kamandar Dezfouli, R. Gordon, and S. Hughes, Modal theory of modified spontaneous emission of a quantum emitter in a hybrid plasmonic photonic-crystal cavity system, Phys. Rev. A **95**, 013846 (2017).

[28] J. N. Liu, Q. Huang, K. K. Liu, S. Singamaneni, and B. T. Cunningham, Nanoantenna-microcavity hybrids with highly cooperative plasmonic-photonic coupling, Nano Lett. **17**, 7569 (2017).

[29] M. Palstra Isabelle, M. Doeleman Hugo, and A. F. Koenderink, Hybrid cavity-antenna systems for quantum optics outside the cryostat? Nanophotonics **8**, 1513 (2019).

[30] M. Frimmer and A. F. Koenderink, Superemitters in hybrid photonic systems: A simple lumping rule for the local density of optical states and its breakdown at the unitary limit, Phys. Rev. B **86**, 235428 (2012).

[31] Y.-C. Liu, X. Luan, H.-K. Li, Q. Gong, C. W. Wong, and Y.-F. Xiao, Coherent Polariton Dynamics in Coupled Highly Dissipative Cavities, Phys. Rev. Lett. **112**, 213602 (2014).

[32] P. Peng, Y. C. Liu, D. Xu, Q. T. Cao, G. Lu, Q. Gong, and Y. F. Xiao, Enhancing Coherent Light-Matter Interactions through Microcavity-Engineered Plasmonic Resonances, Phys. Rev. Lett. **119**, 233901 (2017).

[33] X. Xiong, Y. Lai, D. Clarke, N. Kongsuwan, Z. Dong, P. Bai, C. E. Png, L. Wu, and O. Hess, Control of plexcitonic strong coupling via substrate-mediated hotspot nanoengineering, Adv. Opt. Mater. **10**, 2200557 (2022).

[34] C. Tserkezis, N. A. Mortensen, and M. Wubs, How nonlocal damping reduces plasmon-enhanced fluorescence in ultranarrow gaps, Phys. Rev. B **96**, 085413 (2017).

[35] R. Liu, Z. K. Zhou, Y. C. Yu, T. Zhang, H. Wang, G. Liu, Y. Wei, H. Chen, and X. H. Wang, Strong Light-Matter Interactions in Single Open Plasmonic Nanocavities at the Quantum Optics Limit, Phys. Rev. Lett. **118**, 237401 (2017).

[36] J. Cuerda, F. J. Garcia-Vidal, and J. Bravo-Abad, Spatio-temporal modeling of lasing action in core-shell metallic nanoparticles, ACS Photonics **3**, 1952 (2016).

[37] T. V. Shahbazyan, Mode volume, energy transfer, and spaser threshold in plasmonic systems with gain, ACS Photonics **4**, 1003 (2017).

[38] Y.-W. Lu, W.-J. Zhou, Y. Li, R. Li, J.-F. Liu, L. Wu, and H. Tan, Unveiling atom-photon quasi-bound states in hybrid plasmonic-photonic cavity, Nanophotonics **11**, 3307 (2022).

[39] Y.-W. Lu, J.-F. Liu, Z. Liao, and X.-H. Wang, Plasmonic-photonic cavity for high-efficiency single-photon blockade, Sci. China Phys. Mech. Astron. **64**, 274212 (2021).

[40] M. O. Scully and M. S. Zubairy, *Quantum Optics* (Cambridge University Press, Cambridge, UK, 1999).

[41] D. Pellegrino, D. Balestri, N. Granchi, M. Ciardi, F. Intonti, F. Pagliano, A. Y. Silov, F. W. Otten, T. Wu, K. Vynck, P. Lalanne, A. Fiore, and M. Gurioli, Non-Lorentzian Local Density of States in Coupled Photonic Crystal Cavities Probed by Near- and Far-Field Emission, Phys. Rev. Lett. **124**, 123902 (2020).

[42] I. Medina, F. J. García-Vidal, A. I. Fernández-Domínguez, and J. Feist, Few-Mode Field Quantization of Arbitrary Electromagnetic Spectral Densities, Phys. Rev. Lett. **126**, 093601 (2021).

[43] H. Haken, *Laser Light Dynamics*, Vol. 2 (North Holland, Netherlands, 1985).

[44] Y.-W. Lu, J.-F. Liu, R. Li, H. Tan, and Y. Li, Fano effect induced giant and robust enhancement of photon correlations in cavity qed systems, Opt. Lett. **47**, 3411 (2022).

[45] E. del Valle and F. P. Laussy, Regimes of strong light-matter coupling under incoherent excitation, Phys. Rev. A **84**, 043816 (2011).

[46] R. Sáez-Blázquez, J. Feist, A. I. Fernández-Domínguez, and F. J. García-Vidal, Enhancing photon correlations through plasmonic strong coupling, Optica **4**, 1363 (2017).

[47] M. Ramezani, A. Halpin, A. I. Fernández-Domínguez, J. Feist, S. R.-K. Rodriguez, F. J. Garcia-Vidal, and J. Gómez Rivas, Plasmon-exciton-polariton lasing, Optica **4**, 31 (2017).

[48] Y.-W. Lu, J.-F. Liu, R. Liu, R. Su, and X.-H. Wang, Quantum exceptional chamber induced by large nondipole effect of a quantum dot coupled to a nano-plasmonic resonator, Nanophotonics **10**, 2431 (2021).

[49] H. Qiao, K. A. Abel, F. C. J. M. van Veggel, and J. F. Young, Exciton thermalization and state broadening contributions to the photoluminescence of colloidal PbSe quantum dot films from 295 to 4.5 K, Phys. Rev. B **82**, 165435 (2010).

[50] G. Chen, Y.-C. Yu, X.-L. Zhuo, Y.-G. Huang, H. Jiang, J.-F. Liu, C.-J. Jin, and X.-H. Wang, Ab initio determination of local coupling interaction in arbitrary nanostructures: Application to photonic crystal slabs and cavities, Phys. Rev. B **87**, 195138 (2013).

[51] M. W. McCutcheon and M. Lonar, Design of a silicon nitride photonic crystal nanocavity with a quality factor of one million for coupling to a diamond nanocrystal, Opt. Express **16**, 19136 (2008).

[52] S. Franke, M. Richter, J. Ren, A. Knorr, and S. Hughes, Quantized quasinormal-mode description of nonlinear cavity-QED effects from coupled resonators with a Fano-like resonance, Phys. Rev. Res. **2**, 033456 (2020).

[53] Y.-F. Xiao, Y.-C. Liu, B.-B. Li, Y.-L. Chen, Y. Li, and Q. Gong, Strongly enhanced light-matter interaction in a hybrid photonic-plasmonic resonator, Phys. Rev. A **85**, 031805(R) (2012).

[54] H. Choi, M. Heuck, and D. Englund, Self-Similar Nanocavity Design with Ultrasmall Mode Volume for Single-Photon Nonlinearities, Phys. Rev. Lett. **118**, 223605 (2017).

[55] E. Waks and D. Sridharan, Cavity QED treatment of interactions between a metal nanoparticle and a dipole emitter, Phys. Rev. A **82**, 043845 (2010).

[56] M. L. Andersen, S. Stobbe, A. S. Sørensen, and P. Lodahl, Strongly modified plasmonmatter interaction with mesoscopic quantum emitters, Nat. Phys. **7**, 215 (2011).

[57] M. Paul, F. Olbrich, J. Höschele, S. Schreier, and P. Michler, Single-photon emission at 1.55 μm from MOVPE-grown InAs quantum dots on InGaAs/GaAs metamorphic buffers, Appl. Phys. Lett. **111**, 033102 (2017).

[58] T. Müller, J. Skiba-Szymanska, A. B. Krysa, J. Huwer, M. Felle, M. Anderson, R. M. Stevenson, J. Heffernan, D. A. Ritchie, and A. J. Shields, A quantum light-emitting diode for the standard telecom window around 1550 nm, Nat. Commun. **9**, 862 (2018).

[59] M. I. Kolobov, L. Davidovich, E. Giacobino, and C. Fabre, Role of pumping statistics and dynamics of atomic polarization in quantum fluctuations of laser sources, Phys. Rev. A **47**, 1431 (1993).

[60] A. Jann and Y. Ben-Aryeh, Quantum-noise reduction in semiconductor lasers, J. Opt. Soc. Am. B **13**, 761 (1996).

[61] I. E. Protsenko, A. V. Uskov, E. C. André, J. Mørk, and M. Wubs, Quantum Langevin approach for superradiant nanolasers, New J. Phys. **23**, 063010 (2021).

[62] N. V. Larionov and M. I. Kolobov, Quantum theory of a single-emitter nanolaser, Phys. Rev. A **88**, 013843 (2013).

[63] R. Verre, D. G. Baranov, B. Munkhbat, J. Cuadra, M. Kall, and T. Shegai, Transition metal dichalcogenide nanodisks as high-index dielectric mie nanoresonators, Nat. Nanotechnol. **14**, 679 (2019).

[64] V. Karanikolas, I. Thanopulos, and E. Paspalakis, Strong interaction of quantum emitters with a WS2 layer enhanced by a gold substrate, Opt. Lett. **44**, 2049 (2019).

[65] D. Tamascelli, A. Smirne, S. F. Huelga, and M. B. Plenio, Nonperturbative Treatment of Non-Markovian Dynamics of Open Quantum Systems, Phys. Rev. Lett. **120**, 030402 (2018).

[66] E. V. Denning, J. Iles-Smith, and J. Mork, Quantum light-matter interaction and controlled phonon scattering in a photonic Fano cavity, Phys. Rev. B **100**, 214306 (2019).

[67] T. Gruner and D. G. Welsch, Green-function approach to the radiation-field quantization for homogeneous and inhomogeneous Kramers-Kronig dielectrics, Phys. Rev. A **53**, 1818 (1996).